Universidade de Aveiro Departamento de Física,
2020

João Pedro Dias Rodrigues

A Study of possibilities beyond the Standard Model

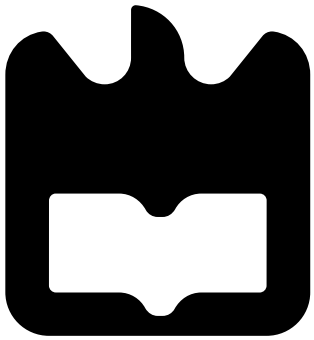

o júri / the jury

presidente

Margarida Facão
Professora Auxiliar do Departamento de Física da Universidade de Aveiro

vogais

António Morais
Investigador Pos-doc do Departamento de Física da Universidade de Aveiro

Nuno Castro?
Professor at the University of Minho. Researcher at LIP and ATLAS experiment at CERN.

agradecimentos / acknowledgements

Honestamente acho que isto vai ter que ser escrito antes da entrega

Honestly this will be written in english translated poorly from above :)

Resumo Esta parte esta em pt

Abstract This part will be in English

Contents

List of Figures

List of Tables

1 Introduction

Without a doubt the conventional theory which is to be used in the study of particle physics is the Standard Model (SM) of particle physics. This is simply due to the fact that the SM has thus far the best descriptor for the experimentally observed spectra of particles and their interactions at all current probable scales.

The history of the SM is a interesting one and with it's formulation scientists achieved a complete theory that combines three of the four fundamental forces of nature in a very well motivated framework, making it one of the most monumental achievements in physics.

It's final piece was finally discovered in 2012. This discovery validated the mass generation mechanism of all subatomic particles as stemming spontaneous symmetry breaking. In the SM the broken symmetries are that of the the $SU(2)_L \times U(1)_Y$ into the electromagnetic symmetry $U(1)_{EM}$.

Is it safe to say that the SM is more of a empirical model given how we set it's couplings and the such and mention it doesn't account for GUT for example?

However, despite all these successes the SM still lacks a strong theoretical explanation for several experimental observations. Firstly, the SM can not account for one of the most important cosmological discoveries of the century, observed trough gravitational lensing, the existence of dark matter. This is a fundamental flaw since the SM lacks a possible dark matter candidate, or dark particle.

Secondly, the SM lacks any justification for the existence of baryon asymmetry in the universe, i.e. why is the universe primarily made of matter rather than anti-matter. Although note that the Electroweak baryogenesis (EWBG) remains a theoretically possible and experimentally testable in future? scenario for explaining the cosmic baryon asymmetry, a scenario viable in the SM framework is it? what about CP violation?.

As its name suggests, EWBG refers to a mechanism that produces an asymmetry in the density of baryons decaying during the electroweak phase transition. As any of this been tested by GW experiments?. This puts some requirements on the composition of the universe but would imply that all matter anti-matter asymmetry is created during the time when the Higgs field is settling into it's new vacuum expectation value (VEV).

Thirdly, the SM has peculiar oddities in the fermion sector in the form of unjustified mass and mixing hierarchies. This is usually refereed to as the *flavour problem* and is considered a big drawback of the SM. Specifically, we observe the top quark to be five order of magnitudes heavier the up quark, and eleven orders of magnitude than the observed neutrino masses. These high differences are thought to be too large to be simply "nature", so a mechanism that would justify such gap is a desired property of most Beyond the Standard Model frameworks.

Fourth, note neutrino masses are not included in the SM. Although there are precise oscillation measurements that measure masses in the eV range with precise mixing in between 3 different generations of neutrinos.

These are just some of the typical justifications given to explore possible beyond the Standard Model (BSM) scenarios. The holy grail of which would be a model that include all these problems in a properly motivated framework that addresses these and many more cosmological, gravitational, and phenomenological problems.

However as of late the research in possible BSM as become harder. Given that the available space for new physics gets reduced by each successful experiment. Chief among these experiments is the Large Hadron Collider (LHC), whose large amount of collect data over these past years is setting more and more stringent bounds on viable parameter spaces

of popular BSM scenarios. And as available space for new physics decreases it becomes more challenging to reveal remaining space without falling within the possibility of fine tuning our model.

How to properly explain what fine tunning is?

Note, one of the reasons the SM is so prevalent is that it has shown increasingly puzzling consistence with some measurements that were initial believed to be a possible gateway to new physics. Thus the search continues for hints at possible directions to complete the SM. I should mention flavour changing and how the SM needs a very strange matrix for that to happen

Conventionally, BSM searches in these multi-dimensional parameter spaces have often been made in large computer-clusters with use of several weeks of computational time trough simple Monte-Carlo methods. Although this is the basis of the work presented here a effort was made to incorporate new machine learning routines trough the initial building of smaller learning sets trough conventional methods. Unfortunately this wasn't accomplished in this work due to the expectational setbacks felt this year.

During this work we shall do a small expedition into possible BSM scenarios. To begin we discuss possible extensions of scalar sectors that can be embedded into the SM while also examining the consequences of those addition in the other sectors. Note while the minimally structure of the Higgs sector postulated by the SM is not a immediate contradiction of measurements. It is not manifestly required by the data. And in fact a extended scalar sector is often desired.

This is done as a exercise to observe if such additions are viable despite the relatively tight bounds on Higgs boson couplings to SM gauge boson and heavy fermions. how much should I mention of the 3HDM and the BLSM in the introduction?

We give a higher repute to the Higgs Sector since fermion masses and mixing patterns relate often to the specific structure of the Higgs sector. Also the addition of new scalars offer a large playground for colliders and often the inclusion of new neutrino physics.

After our analysis of a simple unitarity extension is done we'll move on to more complex models with several Higgs Doublets, specifically we'll move to a model containing 3 of these, the 3HDM Model.

These models with more than one Higgs doublet also addresses the observed charge parity CP violation. with the drawback of potentially having large FLavor Changing Neutral Currents (FCNCs). These FCNCs are undesirable at least in large number given observations, altough multiple Higgs Doublets could include these diagrams at tree-level, making them very problematic.

In conclusion two particular multi-Higgs models will be presented in this work a phenomenological study of a 3 Higgs Doublet model (3HDM) with softly broken $\mathrm{U}(1)_(1) \times Z_2$ symmetry and a simple Unitarity ($U(1)$) extension of the SM based on the apparent Baryon minus Lepton symmetry (BLSM) model. We'll investigate what can be learned from these models and what other physical experiments constrict them.

2 The Standard Model of Particle Physics

To pave the way for our future studies we present the SM. Complete with a brief overview of it's mechanisms and a historical introduction. Has stated, it is hard to question the validity of the SM as a successful approximate framework with whom to describe the phenomenology of Particle Physics up to the largest energy scales probed by collider measurements so far. The SM was proposed in the sixties by Glashow, Salam and Weinberg and since it has been extensively tested. Both in contemporary direct searches for new physics and indirect probes via e.g. flavour anomalies and precise electroweak parameter measurements in proton-electron collisions the SM and as said, it's been consistent with most to date.

The path to the formulation of the SM came from previous principles relating to symmetries in nature, specificity symmetry in physical laws. In fact much in modern physics can be attributed to Emmy Noether. Who deduced trough her first theorem that if the action in a system is invariant under some group of transformations (symmetry), then there exist one or more conserved quantities (constants of motion) which are associated to these transformations.

This led to the fundamental question behind the SM. Is it possible that upon imposing to a given Lagrangian the invariance under a certain group of symmetries to reach a given form of the dynamics. These dynamics would be particle interactions and this train of thought led to Quantum Electrodynamics (QED).

We can quote Salam and Ward:

"Our basic postulate is that it should be possible to generate strong, weak and electromagnetic interaction terms (with all their correct symmetry properties and also with clues regarding their relative strengths) by making local gauge transformations on the kinetic energy terms in the free Lagrangian for all particles."

We are glossing over a lot of complexity here, and for the SM to be truly new concepts had to be introduced. In the case of weak interactions the presence of very heavy weak gauge bosons require the new concept of spontaneous breakdown of the gauge symmetry and the Higgs mechanism. Also, the concept of asymptotic freedom played a crucial role to describe perturbatively the strong interaction at short distances.

2.1 Internal symmetry and components of the Standard Model

The Standard Model spectra after the process of Spontaneous Symmetry breaking (SBB) is composed by, first, the weak force carriers, gauge bosons $W^{\pm}$ and Z, and the photon γ, the electromagnetic interaction messenger and finally the strong force mediators, the gluons, g, as well, of course, by the matter particles, the quarks and leptons.

Fermions and quarks are organized in three generations each, with 2 pairs by each generation leading to 6 different particles for each family. For quarks we have the up and down for the first generation, charm and strange for the second as well as top and bottom for the third one. Similarly, there are 6 types of leptons, the charged ones, electron, muon and tau, and the associated neutrinos. These are represented in different manners, being that the quarks are represented by the letters (u, d, c, s, t, b) while leptons as $(e, \nu_e, \mu, \nu_\mu, \tau, \nu_\tau)$.

However we have not yet explained how such states have acquired their masses and quantum numbers, such as colour and electric charge. To show this, we start by presenting the

symmetry group the SM originates from,

$$\mathrm{SU(3)_c \times SU(2)_L \times U(1)_Y} \quad . \tag{1}$$

Here we have see the $\mathrm{SU(3)_c}$ group corresponding to quantum chromodynamics (QCD) responsible for the strong force. We'll see this group remains unbroken, while on the other hand we have the $\mathrm{SU(2)_L \times U(1)_Y}$ group that will be broken by the Higgs mechanism into $\mathrm{U(1)_Q}$. Each particle stems from a field that is charged in a particular manner on each of these groups, making the charge triplets we will come to later define.

Fermions are half integer spin particles most of which have electrical charge (except the neutrinos). While quarks interact via the weak, electromagnetic and strong forces, the charged leptons only feel the electromagnetic and weak forces and the neutrinos are weakly interacting.

A physical fermion is composed of a left-handed and a right-handed field. While the left transform as $SU(2)_L$ doublets and can be written as,

$$L^i = \begin{pmatrix} \nu_{e_L} \\ e_L \end{pmatrix}, \begin{pmatrix} \nu_{\mu_L} \\ \mu_L \end{pmatrix}, \begin{pmatrix} \nu_{\tau_L} \\ \tau_L \end{pmatrix} \quad \text{and} \quad Q^i = \begin{pmatrix} u_L \\ d_L \end{pmatrix}, \begin{pmatrix} c_L \\ s_L \end{pmatrix}, \begin{pmatrix} t_L \\ b_L \end{pmatrix} \quad , \tag{2}$$

where the i index stands for generation, the latter are $\mathrm{SU(2)_L}$ singlets and can be simply represented as

$$e^i_R = \{e_R, \mu_R, \tau_R\}, \quad u^i_R = \{u_R, c_R, t_R\}, \quad d^i_R = \{d_{e_R}, s_{e_R}, b_{e_R}\} \quad , \tag{3}$$

note also that the quarks form triplets of $SU(3)_C$ whereas leptons are colour singlets. The Higgs boson also emerges from an $SU(2)_L$ doublet with the form,

$$H = \begin{pmatrix} \phi^1 + \, i \, \phi^2 \\ \phi^3 + \, i \, \phi^4 \end{pmatrix} \quad , \tag{4}$$

2.2 Fields and Lagrangian

The full set of gauge quantum numbers in the SMs original fields is given in tables 1 and 2.

Table 1: Gauge bosons and Scalar fields in the SM

Fields	Spin 0 field	Spin 1 Field	$SU(3)_C \times SU(2)_L \times U(1)_Y$
Gluons	$\times$	g	(8,1,0)
A bosons	$\times$	A^i	(1,3,0)
B bosons	$\times$	B	(1,1,0)
Higgs field	$(\phi^{\pm}, \phi^0)$	$\times$	(1,2,1)

Table 2: Fermion field dimensions in the SM

Fields	Spin $\frac{1}{2}$ Field	$SU(3)_C \times SU(2)_L \times U(1)_Y$
Quarks (3 gen.)	$Q = (u_L, d_L)$	$(3, 2, \frac{1}{3})$
	u_R	$(3, 1, \frac{4}{3})$
	d_R	$(3, 1, -\frac{2}{3})$
Leptons (3 gen.)	$(L = (\nu_{e_L}, e_L)$	$(1, 2, -1)$
	e_R	$(1, 1, -2)$

The color charge, weak isospin number and the hypercharge are given by their ordered entries in each triplet (seen in the last column of the tables 1 and 2). Given this content we can then write a Lagrangian invariant under transformations of the $SU(3) \times SU(2) \times U(1)$ as.

$$\begin{aligned}\mathcal{L}_{SM} \quad = \quad & (D_\mu H)^\dagger (D^\mu H) - V(HH^\dagger) - \frac{1}{4} F^i_{\mu\nu} F^{i,\mu\nu} - \frac{1}{4} B_{\mu\nu} B^{\mu\nu} \\ & + \overline{L^i_L}(i\gamma^\mu D_\mu) L^i_L + \overline{Q^i_L}(i\gamma^\mu D_\mu) Q^i_L + \overline{L^i_R}(i\gamma^\mu D_\mu) L^i_R + \overline{Q^i_R}(i\gamma^\mu D_\mu) Q^i_R \\ & - [y^d_{jk} \overline{Q}^j_L d^k_R H + y^u_{jk} \overline{Q}^j_L u^k_R \tilde{H} + y^e_{jk} \overline{L}^j e^k_R H + h.c.] \quad ,\end{aligned} \tag{5}$$

where $\tilde{H} = i\sigma_2 H$. At the Lagrangian level, gauge interactions are introduced by the gauge covariant derivative, D_μ, as,

$$D_\mu = \partial_\mu - i g_S \tau^a G^a_\mu - i g T^i A^i_\mu - i g' Y B_\mu \quad , \tag{6}$$

where $\tau^a = \frac{\lambda_a}{2}$, $(a = 1, ..., 8)$ are the generators of $SU(3)_c$, $T_i = \frac{\sigma_i}{2}$, $(i = 1, 2, 3)$ are the generators of $SU(2)_L$ and Y is the generator of $U(1)_Y$ Here the symbols λ_a and σ_i represent the Gell-Mann and Pauli matrices respectively (see appendix). Add later if there is space.

In the first line of Eq. (5), the first term represents the interactions of gauge bosons with the Higgs field and the second term is the scalar potential associated to the said field. The second line represents the gauge-kinetic terms and gauge boson self interactions. The third line describes the fermion kinetic terms as well as the interactions among fermions and gauge bosons. Finally, the last line shows the Yukawa interactions between the Higgs and the fermions. It is due to the Yukawa interactions that the SM fermions acquire their masses once the electro-weak (EW) symmetry is broken, as we will later see.

From Eq. 6 we will present how the Generators A^i_μ and B_μ give rise to the weakly interacting vector bosons $W^\pm$ and Z^0 and the electromagnetic vector boson γ. Contrary to the color sector, where the eight generators G^a_μ simply correspond to eight gluons g a mediating strong interactions.

As previously mentioned it is trough the definition of this covariant derivate that we not only impose the invariance under the gauge transformations, but also impose the interaction of charged fields trough the respective gauge bosons.

2.3 The Higgs mechanism and the mass generation of the Gauge bosons

From what was defined above, we can now study the SSB of $\mathrm{SU(2)_L \times U(1)_Y \rightarrow U(1)_{EW}}$ trough the Higgs Mechanism. Enabling us to find the real physical states of the gauge bosons and the origin of their mass. Let us then consider the part of the Lagrangian containing the

scalar covariant derivatives as defined in eq. (5) , the scalar potential and the gauge-kinetic terms:

$$\mathcal{L}_{gauge} = (D_\mu H)^\dagger (D_\mu H) - V(HH^\dagger) - \frac{1}{4} F^i_{\mu\nu} F^{i,\mu\nu} - \frac{1}{4} B_{\mu\nu} B^{\mu\nu} \quad , \tag{7}$$

The elements of this sector are defined as,

$$V(HH^\dagger) = \mu^2 H^\dagger H + \lambda (H^\dagger H)^2 \quad , \tag{8}$$

$$F^i_{\mu\nu} = \partial_\mu A^i_\nu - \partial_\nu A^i_\mu + g \epsilon_{ijk} A^j_\mu A^k_\nu \quad , \tag{9}$$

In this formulation the constants g and g' are the gauge couplings of the groups $SU(2)_L$ and $U(1)_Y$. We expect a phase shift to occur, namely one that ensures $\mu^2 < 0$ and the VEV we are expected to find then takes the form of,

$$(H^\dagger H) = \frac{-\mu^2}{2\lambda} = \frac{1}{2} v \quad , \tag{10}$$

The VEV is experimentally messured to be $v \approx 246$ GeV. The vacuum can be aligned in such a way that we have,

$$H_{min} = \frac{1}{\sqrt{2}} \begin{pmatrix} 0 \\ v \end{pmatrix} \quad . \tag{11}$$

This vacuum will break the $SU(2)_L \times U(1)_Y$ symmetry down to $U(1)_Q$. this means that in the beginning there are four generators, which are $T^{1,2,3}$ and Y, and after the breaking we are solely left with one unbroken combination that is $Q = (T^3 + 1/2)$. This means that in total we will have three broken generators, thus, from Goldstone Theorem, there will be three massless particles.

As we have seen for the abelian Higgs model, the Goldstones modes can be parametrized as phases in the field space and then can be "rotated away" in the physical basis, leaving us with a single physical massive scalar, the Higgs boson. Note that, with this transformation we are removing three scalar degrees of freedom. However, they cannot just disappear from the theory and will be absorbed by the massive gauge bosons. In fact, a massless gauge boson contains only two scalar degrees of freedom (transverse polarization). Meanwhile, a massive vector boson has two transverse and a longitudinal polarization, i.e., three scalar degrees od freedom. So, as we discussed above, while before the breaking of the EW symmetry we have four massless gauge bosons, after the breaking we are left with three massive ones. This means that there are three extra scalar degrees of freedom showing up in the gauge sector. It is then commonly said that the goldstone bosons are "eaten" by the massive gauge bosons and the total number of scalar degrees of freedom in the theory is preserved. Therefore, without loss of generality, we can rewrite the Higgs doublet as

$$\begin{pmatrix} G_1 + iG_2 \\ v + h(x) + iG_3 \end{pmatrix} = H(x) \to H(x) = \frac{1}{\sqrt{2}} \begin{pmatrix} 0 \\ v + h(x) \end{pmatrix} \quad . \tag{12}$$

Once the Higgs doublet acquires a VEV, the Lagrangian (7) can be recast as:

$$\begin{aligned} \mathcal{L}' =& \frac{1}{2} \partial_\mu h \partial^\mu h - \frac{1}{2} (2v^2 \lambda) h^2 - \frac{1}{4} F^i_{\mu\nu} F^{i,\mu\nu} - \frac{1}{4} B_{\mu\nu} B^{\mu\nu} \\ &+ \frac{1}{8} v^2 g^2 (A^1_\mu A^{1,\mu} + A^2_\mu A^{2,\mu}) + \frac{1}{8} v^2 (g^2 A^3_\mu A^{3,\mu} + g'^2 B_\mu B^\mu - 2 g^2 g'^2 A^3_\mu B^\mu) \quad , \end{aligned} \tag{13}$$

A few things become obvious first, we have a lot of mass terms most stemming from the squared gauge fields and a lonesome squared mass term belonging to the real scalar field we know to be the Higgs field. This makes the Higgs boson mass in the SM to be given by,

$$M_h = (2v^2\lambda) \quad . \tag{14}$$

To obtain masses for the gauge bosons we need to rotate the gauge fields to a basis where the mass terms are diagonal. First, it is straightforward to see that the electrically charged eigenstates are given by

$$W_\mu^\pm = \frac{1}{\sqrt{2}}(A_\mu^{(1)} \pm iA_\mu^{(2)}) \quad , \tag{15}$$

meaning that the mass of the W bosons is,

$$M_{W^\pm} = \frac{1}{2}vg \quad . \tag{16}$$

The situation becomes a bit more complicated for the second term in (13) due to a mixing between A_μ^3 and B_μ. In the gauge eigenbasis the mass terms read

$$\begin{pmatrix} A_\mu^3 & B_\mu \end{pmatrix} \cdot \frac{1}{4}\nu^2 \begin{pmatrix} g^2 & -gg' \\ -gg' & g'^2 \end{pmatrix} \cdot \begin{pmatrix} A_\mu^3 \\ B_\mu \end{pmatrix} \quad , \tag{17}$$

which can be diagonalized to obtain

$$\begin{pmatrix} A_\mu & Z_\mu \end{pmatrix} \begin{pmatrix} 0 & 0 \\ 0 & \frac{1}{2}v\sqrt{g^2+g'^2} \end{pmatrix} \begin{pmatrix} A^\mu \\ Z^\mu \end{pmatrix} \quad , \tag{18}$$

we identify the eigenvector associated to the eigenvalue 0 to the photon and the massive one, $M_Z = \frac{1}{2}v\sqrt{g^2+g'^2}$, to the Z boson. Such eigenvectors can be written as

$$A_\mu = \cos(\theta_\omega)B_\mu + \sin(\theta_\omega)A_\mu^3 \quad , \tag{19}$$

$$Z_\mu = -\sin(\theta_\omega)B_\mu + \cos(\theta_\omega)A_\mu^3 \quad , \tag{20}$$

where θ_w is the so called Weinberg mixing angle and is defined as

$$\cos(\theta_\omega) = \frac{g}{\sqrt{g^2+g'^2}} \quad , \tag{21}$$

thus clearly showing the massless photon along with a massive Z boson with mass $M_Z = \frac{1}{2}\nu\sqrt{g^2+g'^2}$. So we conclude our exploration of the electroweak sector with all the correct massive spectrum observed and its origin discussed.

2.4 The fermion sector on the Standard Model

In order to generate mass for the fermions we can have a closer look at the last line in eq. (5). If we replace the Higgs by the shift in Eq. (12) we get,

$$\begin{aligned}
\mathcal{L}_y = & y^d \begin{pmatrix} \overline{u_L} & \overline{d_L} \end{pmatrix} d_R \begin{pmatrix} 0 \\ v+h(x) \end{pmatrix} + y^s \begin{pmatrix} \overline{c_L} & \overline{s_L} \end{pmatrix} s_R \begin{pmatrix} 0 \\ v+h(x) \end{pmatrix} \\
& + y^b \begin{pmatrix} \overline{t_L} & \overline{b_L} \end{pmatrix} b_R \begin{pmatrix} 0 \\ v+h(x) \end{pmatrix} + y^u \begin{pmatrix} \overline{u_L} & \overline{d_L} \end{pmatrix} d_R \begin{pmatrix} v+h(x) \\ 0 \end{pmatrix} \\
& + y^c \begin{pmatrix} \overline{c_L} & \overline{s_L} \end{pmatrix} d_R \begin{pmatrix} v+h(x) \\ 0 \end{pmatrix} + y^t \begin{pmatrix} \overline{t_L} & \overline{b_L} \end{pmatrix} t_R \begin{pmatrix} v+h(x) \\ 0 \end{pmatrix} \\
& + y^e \begin{pmatrix} \overline{\nu_{e_L}} & \overline{e_L} \end{pmatrix} e_R \begin{pmatrix} 0 \\ v+h(x) \end{pmatrix} + y^\mu \begin{pmatrix} \overline{\nu_{\mu_L}} & \overline{\mu_L} \end{pmatrix} \mu_R \begin{pmatrix} 0 \\ v+h(x) \end{pmatrix} \\
& + y^\tau \begin{pmatrix} \overline{\nu_{\tau_L}} & \overline{\tau_L} \end{pmatrix} \tau_R \begin{pmatrix} 0 \\ v+h(x) \end{pmatrix} + h.c \quad ,
\end{aligned} \tag{22}$$

Further expansion of these terms would result in terms like *e.g.* in the electron's case,

$$\mathcal{L}_{y_e} = y^e \, v \, (\overline{e_L} e_R + \overline{e_R} e_L) + y^e h(x) \, (\overline{e_L} e_R + \overline{e_R} e_L) \quad , \tag{23}$$

where since the electron field is written as,

$$e = \begin{pmatrix} e_L \\ e_R \end{pmatrix} \quad , \tag{24}$$

meaning the first terms in (23) equate to electron mass terms as, $m_e \overline{e} e$ and the second terms represent interaction between the electron and the Higgs boson. This is how the Higgs mechanism generates the mass to all of the fermionic sector except neutrinos due to the SM not containing right handed neutrinos. The absence of neutrino masses contradicts experimental observations. Note, that each field shares the same conserved charges and can be grouped in families with increasing masses their masses depend directly on the term hierarchy of the Yukawa terms. Terms of similar shape are generated for quarks as well, in fact for the example of the up and down quarks we can write.

$$M^u_{ij} = Y^u_{ij} \frac{v}{\sqrt{2}} \quad M^d_{ij} = Y^d_{ij} \frac{v}{\sqrt{2}} \tag{25}$$

where M are the mass matrices for the up-type and down-type quarks have been expressed in terms of generic 3×3 complex Yukawa matrices and the v the VEV of the Higgs doublet. It is interesting to consider however that these matrices although trivial to diagonalize are not unique, there for the Yukawa are not uniquely defined and a conclusive fundamental explanation of their origin still does not exist.

As a example it would be simple to find a diagonal yukawa matrix to account for the proper mass terms for the quarks. However including non diagonal terms would lead to tree level FCNCs. Which should be present only present at higher orders of perturbation theory, they must be naturally suppressed at tree-level.

However due to precise quark measurements we can present some constraints on the nature of the Yukawa matrix. Due to the fact that the SM is made to account for the existence of charge parity $\mathcal{CP}$ violation in the form the Cabibbo–Kobayashi–Maskawa (CKM) matrix. Note, although the interactions of quarks are measured with very high precision, a substantial justification for its hierarchical structure still remains unclear. The CKM matrix has its origin in charged currents, these currents lead to patterns when diagonalizing mass matrices and rotating quark spinors to the mass basis. The diagonalization of the real quark states can be performed while leaving space for a generic 3×3 matrix, Y if performed by a set of four bi-unitary matrices, as seen,

$$m^{u}_{diag.} = \frac{v}{\sqrt{2}} \mathrm{U}^{u}_{L} \mathrm{Y} \mathrm{U}^{u\,\dagger}_{R} \tag{26}$$

$$m^{d}_{diag.} = \frac{v}{\sqrt{2}} \mathrm{U}^{d}_{L} \mathrm{Y} \mathrm{U}^{d\,\dagger}_{R} \tag{27}$$

I am having a real hard time explaining the CKM part only affecting the left handed and doing the entire demonstrations I need help

3 B-L-SM Model

Having discussed the Standard Model, we are ready to look at what might lie beyond it. In this chapter we introduce the minimal $U(1)_{B-L}$ extension of the Standard Model named, the B-L-SM Model. This is a model trough which we can explain neutrino mass generation via a simple see-saw mechanism as well as, by virtue of the model containing two new physical particle states, specifically a new Higgs like boson H' and a Z' gauge Boson, other small deviations in electro-weak measurements, namely the $(g-2)_\mu$ anomaly. This refers to the discrepancy between the measured anomalous magnetic moment of the muon. We try to examine how non-collider experiments could limit the study of new Models such as the B-L-SM.

Both the additional bosons are given mass mostly trough the spontaneous breaking of the $U(1)_{B-L}$ symmetry that gives it's name to the Model. This unitary group originates from the promotion of a accidental symmetry present in the SM, the Baryon number (B) minus the Lepton number (L) to a fundamental Abelian symmetry group. This origin for the mass of the referenced bosons means model is already very heavily constricted due to long-standing direct searches in the Large Hadron Collide (LHC).

Trough this model we can also address the metastability of the electroweak (EW) vacuum in the SM trough the addition of the new scalar. Allowing for Higgs stabilization up to the plank scale with a the new Higgs starting from few hundred of GeVs.

The presence of the complex SM-singlet field, χ, interacting with a Higgs doublet typically enhances the strength of EW phase transition potentially converting it into a strong first-order one. Although not covered in this work, the strength of this transition could be analysed to determine a possible gravitational wave spectrum. Such a analysis is of utmost importance given that it could provide a way to detect new physics and confirm or exclude the model without the need for a larger particle collider but instead a sensitive probe also capable of studying gravitational events. This could be pointed to as future work.

The B-L-SM is also easily embedded into higher order symmetry groups like for example the $SO(10)$ or or E_6 , giving this model the ability to be used for the study of Grand Unified Theories (GUT).

The presence of three generations of right-handed neutrinos instead of a arbitrary number of neutrinos is purposely made, ensuring a framework free of anomalies. The mass scale of such neutrinos is established once the $U(1)_{B-L}$ is broken by the VEV, x, of a complex SM-singlet scalar field, χ. This VEV simultaneously gives mass to the corresponding Z' boson and H'.

The cosmological consequences of the B-L-SM formulation are also worth mentioning. First, the presence of an extended neutrino sector implies the existence of a sterile state that can play the role of Dark Matter candidate. These can be completely sterile if stabilized with a $\mathbb{Z}_2$ parity symmetry. Note that the existence of sterile neutrinos can be used to explain the baryon asymmetry via the leptogenesis mechanism.

The goal of this chapter in our work is to present the fundamental theoretical background on the model and a modern precise study of the phenomenological status of the B-L-SM model. As well as trying to use multiple experiments to increasingly narrow down the available parameter space of the model.

3.1 Formulating the model

Essentially, the minimal B-L-SM is a Beyond the Standard Model (BSM) framework containing three new ingredients:

- A new gauge interaction
- Three generations of right handed neutrinos
- A complex scalar SM-singlet.

The first one is well motivated in various GUT scenarios. However a family-universal symmetry such as $U(1)_{B-L}$ being introduced without changing the SM fermion content would lead to chiral anomalies. This translates to a non conservative charged current on some channels involving the $U(1)_{B-L}$. These aren't completely undesired by themselves, since their result would be charge conjugation parity symmetry violation, but this inclusion would lead to processes at tree-level, thus resulting in far too much of these phenomena.

Secondly, as mentioned, a new sector of additional three $U(1)_{B-L}$ charged Majorana neutrinos is essential for anomaly cancellation.

Finally, the SM-like Higgs doublet, H, does not carry neither baryon nor lepton number, this way it does not participate in the breaking of $U(1)_{B-L}$. It is then necessary to introduce a new scalar singlet, χ, solely charged under $U(1)_{B-L}$, whose VEV breaks the $B-L$ symmetry. It is also this breaking scale that generates masses for heavy neutrinos. As mentioned this breaking occurs before the EW breaking.

The particle content and related charges of the minimal $U(1)_{B-L}$ extension of the SM are shown in the table. Note these are similar to the SM as to be expected.

	q_L	u_R	d_R	l_L	e_R	ν_R	H	χ
$SU(3)_c$	3	3	3	1	1	1	1	1
$SU(2)_L$	2	1	1	2	1	1	2	1
$U(1)_Y$	$\frac{1}{6}$	$\frac{2}{3}$	$-\frac{1}{3}$	$-\frac{1}{2}$	-1	0	$\frac{1}{2}$	0
$U(1)_{B-L}$	$\frac{1}{3}$	$\frac{1}{3}$	$\frac{1}{3}$	-1	-1	-1	0	2

Table 3: Quantum fields and their respective quantum numbers in the minimal B-L-SM extension. The last two lines represent the weak and $B-L$ hypercharges

3.1.1 Scalar sector

Given the information seen above and the information we got in the previous chapter, we can begin examining the new Lagrangian terms. Starting by the scalar potential, which now depends on two fields as seen in,

$$V(H,\chi) = \mu_1^2 H^\dagger H + \mu_2^2 \chi^* \chi + \lambda_1 (H^\dagger H)^2 + \lambda_2 (\chi^* \chi)^2 + \lambda_3 \chi^* \chi H^\dagger H \tag{28}$$

This potential must lead to stable vacuum state, for this to be ensured we state that the scalar potential must be bounded from below (BFB), ensuring a global minima. Studying the potential on eq. 28 we deduce the conditions,

$$4\lambda_1\lambda_2 - \lambda_3^2 > 0 \quad , \quad \lambda_1, \lambda_2 > 0 \tag{29}$$

Where the full components of the scalar fields H and χ are given by,

$$H = \frac{1}{\sqrt{2}} \begin{pmatrix} -i\left(\omega_1 - i\omega_2\right) \\ v + (h + iz) \end{pmatrix} \quad \chi = \frac{1}{\sqrt{2}} \left(x + \left(h' + iz'\right)\right) \tag{30}$$

In these equations we can see h and h' representing the radial quantum fluctuations around the minimum of the potential. These will constitute the physical degrees of freedom associated to the H and H'. There are also four Goldstone directions denoted as ω_1, ω_2, z and z' which are absorbed into longitudinal modes of the $W^{\pm}$, Z and Z' gauge bosons once spontaneous symmetry breaking (SSB) takes place. After SSB the associated VEVs take the form,

$$\langle H \rangle = \frac{1}{\sqrt{2}} \begin{pmatrix} 0 \\ v \end{pmatrix} \qquad \langle \chi \rangle = \frac{x}{\sqrt{2}} \tag{31}$$

here, recall v and x are the associated VEVs to each field. From here we can solve the tadpole equations in relation to each of the VEVs as to ensure non-zero minima, we arrive at,

$$v^2 = \frac{-\lambda_2\mu_1^2 + \frac{\lambda_3}{2}\mu_2^2}{\lambda_1\lambda_2 - \frac{1}{4}\lambda_3^2} > 0 \qquad \text{and} \qquad x^2 = \frac{-\lambda_1\mu_2^2 + \frac{\lambda_3}{2}\mu_1^2}{\lambda_1\lambda_2 - \frac{1}{4}\lambda_3^2} > 0 \tag{32}$$

which, when simplified with the bound from bellow conditions yield a simpler set of equations,

$$\lambda_2\mu_1^2 < \tfrac{\lambda_3}{2}\mu_2^2 \qquad \text{and} \qquad \lambda_1\mu_2^2 < \tfrac{\lambda_3}{2}\mu_1^2 \tag{33}$$

Note that although λ_1 and λ_2 must be positive to ensure the correct potential shape, no such conditions exist for the sign of λ_3 , μ_1 and μ_2. However observing equation 33 we can infer that some combinations of signs are impossible, For our studies we decided to leave the

	$\mu_2^2 > 0$ $\mu_1^2 > 0$	$\mu_2^2 > 0$ $\mu_1^2 < 0$	$\mu_2^2 < 0$ $\mu_1^2 > 0$	$\mu_2^2 < 0$ $\mu_1^2 < 0$
$\lambda_3 < 0$	✗	✓	✓	✓
$\lambda_3 > 0$	✗	✗	✗	✓

Table 4: Possible Signs of the potential parameters in (28). While the ✓ symbol indicates the existence of solutions for tadpole conditions (33), the ✗ indicates unstable configurations.

sign of λ_3 positive, choosing a configuration where both μ parameters are negative. This doesn't directly translate to any real physical consequence. These conditions now established we proceed to investigate the physical states of B-L-SM scalar sector. By first, taking the Hessian matrix evaluated at the vacuum value,

$$\mathbf{M}^2 = \begin{pmatrix} 4\lambda_2 x^2 & \lambda_3 vx \\ \lambda_3 vx & 4\lambda_1 v^2 \end{pmatrix} , \tag{34}$$

Moving this matrix to it's physical mass eigen-base, we obtain the following eigenvalues,

$$m_{h_{1,2}}^2 = \lambda_1 v^2 + \lambda_2 x^2 \mp \sqrt{(\lambda_1 v^2 - \lambda_2 x^2)^2 + (\lambda_3 xv)^2} \, , \tag{35}$$

The physical basis vectors h_1 and h_2 can then be related to the original fields of gauge eigenbasis h and h' trough a simple rotation matrix:

$$\begin{pmatrix} h_1 \\ h_2 \end{pmatrix} = \mathbf{O} \begin{pmatrix} h \\ h' \end{pmatrix} . \tag{36}$$

Being that, the rotation matrix is written as,

$$\mathbf{O} = \begin{pmatrix} \cos\alpha_h & -\sin\alpha_h \\ \sin\alpha_h & \cos\alpha_h \end{pmatrix} . \tag{37}$$

Recall that due to the SSB order $x > v$. The precise mixing angle is represented simply by,

$$\tan 2\alpha_h = \frac{|\lambda_3|\, vv'}{\lambda_1 v^2 - \lambda_2 {v'}^2} \tag{38}$$

Although consider it is worth presenting the case of approximate decoupling where, $v/x \ll 1$. In this case scalar masses and mixing angle become particularly simple,

$$\sin\alpha_h \approx \frac{1}{2}\frac{\lambda_3}{\lambda_2}\frac{v}{x} \qquad m^2_{h_1} \approx 2\lambda_1 v^2 \qquad m^2_{h_2} \approx 2\lambda_2 x^2 \tag{39}$$

We will see in the context of our numerical results that for our phenomenologically consistent mass scale these equations serve a valid approximation for most of the points.

3.1.2 Gauge Sector

Moving onto the gauge boson and Higgs kinetic terms in the B-L-SM, consider the following portion of the Lagrangian,

$$\mathcal{L}_{U(1)'s} = |D_\mu H|^2 + |D_\mu \chi|^2 - \frac{1}{4}F_{\mu\nu}F^{\mu\nu} - \frac{1}{4}F'_{\mu\nu}F'^{\mu\nu} - \frac{1}{2}\kappa F_{\mu\nu}F'^{\mu\nu} \tag{40}$$

where $F^{\mu\nu}$ and $F'^{\mu\nu}$ are the standard field strength tensors, respectively for the hypercharge $U(1)_Y$ and B minus L $U(1)_{B-L}$,

$$F_{\mu\nu} = \partial_\mu A_\nu - \partial_\nu A_\mu \qquad \text{and} \qquad F'_{\mu\nu} = \partial_\mu A'_\nu - \partial_\nu A'_\mu \, . \tag{41}$$

written in terms of the gauge fields A_μ and A'_μ, respectively. Given that this is a model with two Unitary groups, without a parity symmetry to prevent it, we must consider the possible mixing in between them. In this work we parametrized this mixing trough a parameter κ.

The Abelian part of the covariant derivative in equation 40 is given by,

$$D_\mu \supset i g_1 Y A_\mu + i g'_1 Y_{\mathrm{B-L}} A'_\mu \, , \tag{42}$$

with g_1 and g'_1 being the $U(1)_Y$ and $U(1)_{B-L}$ the gauge couplings with the Y and $B-L$ charges are specified in Tab. 3. However it is convenient to rewrite the gauge kinetic terms in the canonical form, i.e.

$$F_{\mu\nu}F^{\mu\nu} + F'_{\mu\nu}F'^{\mu\nu} + 2\kappa F_{\mu\nu}F'^{\mu\nu} \to B_{\mu\nu}B^{\mu\nu} + B'_{\mu\nu}B'^{\mu\nu} \, . \tag{43}$$

A generic orthogonal transformation in the field space does not eliminate the kinetic mixing term. So, in order to satisfy Eq. (43) an extra non-orthogonal transformation should be imposed such that Eq. (43) is realized. Taking $\kappa = \sin\alpha$, a suitable redefinition of fields $\{A_\mu, A'_\mu\}$ into $\{B_\mu, B'_\mu\}$ that eliminates κ-term according to Eq. (40) can be cast as

$$\begin{pmatrix} A_\mu \\ A'_\mu \end{pmatrix} = \begin{pmatrix} 1 & -\tan\alpha \\ 0 & \sec\alpha \end{pmatrix} \begin{pmatrix} B_\mu \\ B'_\mu \end{pmatrix} , \tag{44}$$

Note there is a limit without kinitic mixing where $\alpha = 0$. Note that this transformation is generic and valid for any basis in the field space. The transformation (44) results in a modification of the covariant derivative that acquires two additional terms encoding the details of the kinetic mixing, i.e.

$$D_\mu \supset \partial_\mu + i\,(g_Y\, Y + g_B Y\, Y_{B-L})\, B_\mu + i\,(g_{B-L}\, Y_{B-L} + g_{YB}\, Y)\, B'_\mu\,, \tag{45}$$

where the gauge couplings take the form

$$\begin{cases} g_Y = g_1 \\ g_{B-L} = g'_1 \sec\alpha \\ g_{YB} = -g_1 \tan\alpha \\ g_{BY} = 0 \end{cases} , \tag{46}$$

which is the standard convention in the literature. The resulting mixing between the neutral gauge fields including Z' can be represented as follows

$$\begin{pmatrix} \gamma_\mu \\ Z_\mu \\ Z'_\mu \end{pmatrix} = \begin{pmatrix} \cos\theta_W & \sin\theta_W & 0 \\ -\sin\theta_W\cos\theta'_W & \cos\theta_W\cos\theta'_W & \sin\theta'_W \\ \sin\theta_W\sin\theta'_W & -\cos\theta'_W\sin\theta'_W & \cos\theta'_W \end{pmatrix} \begin{pmatrix} B_\mu \\ A^3_\mu \\ B'_\mu \end{pmatrix} \tag{47}$$

where θ_W is the weak mixing angle and θ'_W is defined as

$$\sin(2\theta'_W) = \frac{2 g_{YB}\sqrt{g^2 + g_Y^2}}{\sqrt{(g_{YB}^2 + 16(\frac{x}{v})^2 g_{B-L}^2 - g^2 - g_Y^2)^2 + 4 g_{YB}^2 (g^2 + g_Y^2)}}\,, \tag{48}$$

in terms of g and g_Y being the $SU(2)_L$ and U_Y gauge couplings, respectively. In the physically relevant limit, $v/x \ll 1$, the above expression greatly simplifies leading to

$$\sin\theta'_W \approx \frac{1}{16}\frac{g_{YB}}{g_{B-L}}\left(\frac{v}{x}\right)^2 \sqrt{g^2 + g_Y^2}\,, \tag{49}$$

up to $(v/x)^3$ corrections. In the limit of no kinetic mixing, i.e. $g_{YB} \to 0$, there is no mixture of Z' and SM gauge bosons.

Note, the kinetic mixing parameter θ'_W has rather stringent constraints from Z pole experiments both at the Large Electron-Positron Collider (LEP) and the Stanford Linear Collider (SLC), restricting its value to be smaller than 10^{-3} approximately, which we set as an upper

bound in our numerical analysis. Expanding the kinetic terms $|D_\mu H|^2 + |D_\mu \chi|^2$ around the vacuum one can extract the following mass matrix for vector bosons

$$m_V^2 = \frac{v^2}{4}\begin{pmatrix} g^2 & 0 & 0 & 0 & 0 \\ 0 & g^2 & 0 & 0 & 0 \\ 0 & 0 & g^2 & -g g_Y & -g g_{YB} \\ 0 & 0 & -g g_Y & g_Y^2 & g_Y g_{YB} \\ 0 & 0 & -g g_{YB} & g_Y g_{YB} & g_{YB}^2 + 16\left(\frac{x}{v}\right)^2 g_{B-L}^2 \end{pmatrix} \tag{50}$$

whose eigenvalues read

$$m_A = 0\,, \qquad m_W = \tfrac{1}{2} v g \tag{51}$$

corresponding to physical photon and $W^\pm$ bosons as well as

$$m_{Z,Z'} = \sqrt{g^2 + g_Y^2} \cdot \frac{v}{2}\sqrt{\frac{1}{2}\left(\frac{g_{YB}^2 + 16(\frac{x}{v})^2 g_{\rm BL}^2}{g^2 + g_Y^2} + 1\right) \mp \frac{g_{YB}}{\sin(2\theta'_W)\sqrt{g^2 + g_Y^2}}}\,. \tag{52}$$

for two neutral massive vector bosons, with one of them, not necessarily the lightest, representing the SM-like Z boson. It follows from LEP and SLC constraints on θ'_W, that Eq. (49) also implies that either g_{YB} or the ratio $\frac{v}{x}$ are small. In this limit, Eq. (52) simplifies to

$$m_Z \approx \tfrac{1}{2} v \sqrt{g^2 + g_Y^2} \qquad \text{and} \qquad m_{Z'} \approx 2 g_{B-L} x\,, \tag{53}$$

where the $m_{Z'}$ depends only on the SM-singlet VEV ,x and on the $U(1)_{B-L}$ gauge coupling and will be attributed to a heavy Z' state, while the light Z-boson mass corresponds to its SM value.

3.2 The Yukawa sector

One of the key features of the B-L-SM is the presence of non-zero neutrino masses. In its minimal version, such masses are generated via a type-I seesaw mechanism. The Yukawa Lagrangian of the model reads

$$\mathcal{L}_f = -Y_u^{ij}\overline{q_{\rm Li}} u_{\rm Rj}\widetilde{H} - Y_d^{ij}\overline{q_{\rm Li}} d_{\rm Rj} H - Y_e^{ij}\overline{\ell_{\rm Li}} e_{\rm Rj} H - Y_\nu^{ij}\overline{\ell_{\rm Li}}\nu_{\rm Rj}\widetilde{H} - \frac{1}{2}Y_\chi^{ij}\overline{\nu_{\rm Ri}^c}\nu_{\rm Rj}\chi + \text{c.c.} \tag{54}$$

Notice that Majorana neutrino mass terms of the form $M\overline{\nu_R^c}\nu_R$ would explicitly violate the $U(1)_{B-L}$ symmetry and are therefore not present. In Eq. (54), Y_u, Y_d and Y_e are the 3×3 Yukawa matrices that reproduce the quark and charged lepton sector of the SM, while Y_ν and Y_χ are the new Yukawa matrices responsible for the generation of neutrino masses and mixing. In particular, one can write

$$\mathbf{m}_{\nu_l}^{Type-I} = \frac{1}{\sqrt{2}}\frac{v^2}{x}\mathbf{Y}_\nu^t \mathbf{Y}_\chi^{-1}\mathbf{Y}_\nu\,, \tag{55}$$

for light ν_l neutrino masses, whereas the heavy ν_h ones are given by

$$\mathbf{m}_{\nu_h}^{Type-I} \approx \frac{1}{\sqrt{2}}\mathbf{Y}_\chi x\,, \tag{56}$$

where we have assumed a flavour diagonal basis. Note that the smallness of light neutrino masses imply that either the x VEV is very large or (if we fix it to be at the $\mathcal{O}(TeV)$ scale and $\mathbf{Y}_\chi \sim \mathcal{O}(1)$) the corresponding Yukawa coupling should be tiny, $\mathbf{Y}_\nu < 10^{-6}$. It is clear that the low scale character of the type-I seesaw mechanism in the minimal B-L-SM is *faked* by small Yukawa couplings to the Higgs boson. A more elegant description was proposed in Ref. [**?**] where small SM neutrino masses naturally result from an inverse seesaw mechanism. In this work, however, we will not study the neutrino sector and thus, for an improved efficiency of our numerical analysis of Z' observables, it will be sufficient to fix the Yukawa couplings to $\mathbf{Y}_\chi = 10^{-1}$ and $\mathbf{Y}_\nu = 10^{-7}$ values such that the three lightest neutrinos lie in the sub-eV domain.

3.3 Phenomenological analysis

The numerical results that will be presented in this section were created trough the first generation of a tool developed during the course of this thesis.

The created tool was based on a series of bash and python scripts that would generate a Monte-Carlo type scan trough all the parameter space within the desired orders of magnitude. All points were sequentially checked against the most resent modern constraints stemming from several experiments like the LHC.

So after the generation of a set of couplings and physical constants the very first layer of phenomenological checks is done by `SPheno` which promptly rejects any scenario with tachyonic scalar masses and un-renormalizable quantities.

`SPheno` is a particle spectrum generator code written in Fortran 90. It's emphasis on easy generalisability and speed made it a natural part of our phenomenological analysis. It accepts information about our model's Lagrangian, such as fields, charges and fundamental symmetries, and creates a executable file capable of quickly generating a spectrum file with all details regarding mass, decay and flavour observables information in the standardized SUSY Les Houches accord format.

The Lagrangian information is fed to `SPheno` also in standardized format automatically generated by a Mathematica packaged designed for such purposes called `SARAH`.

After a point completes the first layer, we take information from it's two and three body decays in particular to the Higgs bosons and perform the first test of the Higgs Sector by running a set of Programs called `HiggsBounds` and `HiggsSignals`. These test experimental detection limits for the new scalars and verify if we have a "SM" like Higgs to account for the detected boson.

However the presence of new bosons in the theory can lead to large deviations in EW precision observables. Typically, the most stringent constraints of the scalar sector emerge from the oblique S, T, U parameters, which are also calculated by `SPheno`. Current precision measurements provide the allowed regions,

$$S = 0.02 \pm 0.10\,, \qquad T = 0.07 \pm 0.12\,, \qquad U = 0.00 \pm 0.09 \tag{57}$$

where S-T are 92% correlated, while S-U and T-U are -66% and -86% anti-correlated, respectively. We compare our results with the EW fit in Eq. (57) and require consistency with the best fit point within a 95% C.L. ellipsoid (see Ref. [**?**] for further details about this method). We show in Fig. 1 our results in the ST (left) and TU (right) planes where black points are consistent with EW precision observables at 95% C.L. whereas grey ones lie outside the corresponding ellipsoid of the best fit point and, thus, are excluded in our analysis.

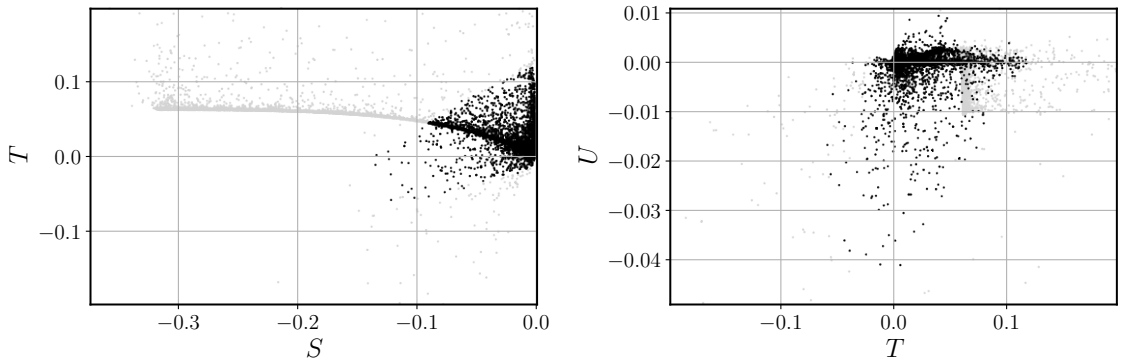

Figure 1: Scatter plots for EW precision observables showing the ST (left) and TU (right) planes. Accepted points lying within a 95% C.L. ellipsoid of the best fit point are represented in black whereas grey points are excluded.

Thus, in a second layer of phenomenological tests, we confront the surviving scenarios, black points in Fig. 1, with collider bounds. In particular, we use `HiggsBounds 4.3.1` [**?**] to apply 95% C.L. exclusion limits on a new scalar particle, h_2, and `HiggsSignals 1.4.0` [**?**] to check for consistency with the observed Higgs boson taking into account all known Higgs signal data. For the latter, we have accepted points whose fit to the data replicates the observed signal at 95% C.L. while the measured value for its mass, $m_{h_1} = 125.10 \pm 0.14$ GeV [**?**], is reproduced within a 3σ uncertainty. The required input data for `HiggsBounds/HiggsSignals` are generated by the `SPheno` output in the format of a SUSY Les Houches Accord (SLHA) [**?**] file. In particular, it provides scalar masses, total decay widths, Higgs decay branching ratios as well as the SM-normalized effective Higgs couplings to fermions and bosons squared (that are needed for analysis of the Higgs boson production cross sections). For details about this calculation, see Ref. [**?**].

On a third layer of phenomenological tests we have studied the viability of the surviving scenarios from the perspective of direct collider searches for a new Z' gauge boson. We have used `MadGraph5_aMC@NLO 2.6.2` [**?**] to compute the Z' Drell-Yan production cross section and subsequent decay into the first and second-generation leptons, i.e. $\sigma\left(pp \to Z'\right) \times B\left(Z' \to \ell\ell\right)$ with $\ell = e,\ \mu$, and then compared our results to the most recent ATLAS exclusion bounds from the LHC runs at the center-of-mass energy $\sqrt{s} = 13$ TeV [**?**]. The `SPheno` SLHA output files were used as parameter cards for `MadGraph5_aMC@NLO`, where the information required to calculate $\sigma\left(pp \to Z'\right) \times B\left(Z' \to \ell\ell(\right)$, such as the Z' boson mass, its total width and decay branching ratios into lepton pairs, is provided.

The lepton anomalous magnetic moments $(g-2)_\ell/2 \equiv a_\ell$ are calculated in `SPheno` at one-loop order. In the B-L-SM, new physics (NP) contributions to a_μ, denoted as $\Delta a_\mu^{\rm NP}$ in what follows, can emerge from the diagrams containing Z' or h_2 propagators. In this article, we study whether the muon anomalous magnetic moment can be totally or partially explained in the model under consideration and all scenarios with an excessive contribution to $\Delta a_\mu^{\rm NP}$ larger than the upper 2σ bound in Eq. (**??**) were rejected.

3.4 Discussion of numerical results

Let us now discuss the phenomenological properties of the B-L-SM model. First, we focus on the current collider constraints and study their impact on both the scalar and gauge sectors.

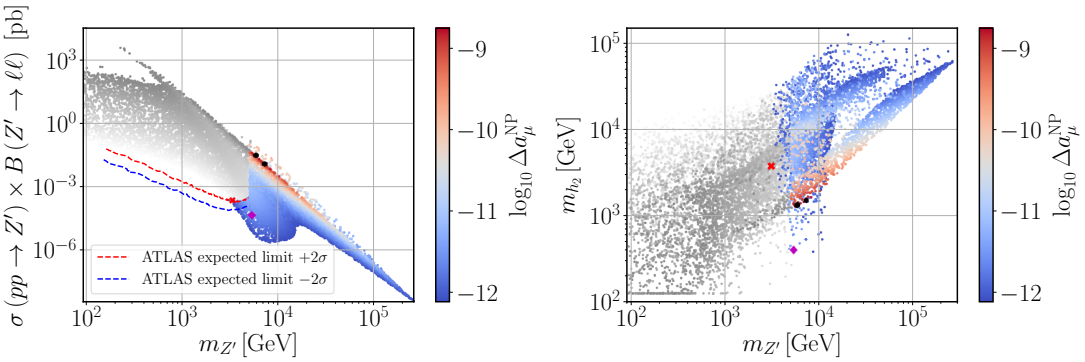

Figure 2: Scatter plots showing the Z' Drell-Yan production cross section times the decay branching ratio into a pair of electrons and muons (left panel) and the new scalar mass m_{h_2} (right panel) as functions of $m_{Z'}$ and the new physics (NP) contributions to the muon Δa_μ anomaly. Coloured points have survived all theoretical and experimental constraints while grey points are excluded by direct Z' searches at the LHC. The region between the two dashed lines represents the current ATLAS expected limit on the production cross section times branching ratio into a pair of leptons at 95% C.L. and is taken from the *Brazilian* plot in Fig. 4 of Ref. [**?**]. The four highlighted points in both panels denote the benchmark scenarios described in detail in Tab. 5.

We show in Fig. 2 the scenarios generated in our parameter space scan (see Tab. **??**) that have passed all theoretical constraints such as boundedness from below, unitarity and EW precision tests, are compatible with the SM Higgs data and where a new visible scalar h_2 is unconstrained by the direct collider searches. On the left panel, we show the Z' production cross section times its branching ratio to the first- and second-generation leptons, $\sigma B \equiv \sigma\,(pp \to Z') \times B\,(Z' \to \ell\ell)$ with $\ell = e, \mu$, as a function of the new vector boson mass and the new physics contribution to the muon anomalous magnetic moment $\Delta a_\mu^{\rm NP}$ (colour scale). On the right panel, we show the new scalar mass as a function of the same observables. All points above the red dashed line are excluded at 95% C.L. by the upper expected limit on Z' direct searches at the LHC by the ATLAS experiment and are represented in grey shades. Darker shades denote *would-be-scenarios* with larger values of $\Delta a_\mu^{\rm NP}$ while the smaller contributions to the muon $(g-2)_\mu/2$ anomaly are represented with the lighter shades. The region between the two dashed lines corresponds to the Z' ATLAS limit with a 2σ uncertainty represented by the yellow band in Fig. 4 of [**?**]. Provided that the observed limit by the ATLAS detector lies within this region we have taken a conservative approach and accepted all points whose σB value lies below the red dashed line (upper limit) in Fig. 2. The blue dashed line, which corresponds to the stricter 2σ lower bound, is only shown for completeness of information. The red cross in our figures signals the lightest Z' found in our scan which we regard as a possible early-discovery (or early-exclusion) benchmark point in the forthcoming LHC runs. Such a benchmark point is shown in the first line of Tab. 5. On the right panel, we notice that the new scalar bosons can become as light as $380 - 400$ GeV, but with Z' masses in the

range of $5 - 9$ TeV. We highlight with a magenta diamond the benchmark point with the lightest Z' boson within this range. This point is shown in the second line of Tab. 5.

$m_{Z'}$	m_{h_2}	x	$\log_{10}\Delta a_\mu^{\rm NP}$	σB	θ'_W	α_h	$g_{\text{B-L}} \simeq g^{\ell\ell Z'}$
3.13	3.72	15.7	-12.1	2.22×10^{-4}	≈ 0	5.67×10^{-5}	0.0976
5.37	0.396	9.10	-11.7	4.23×10^{-5}	2.55×10^{-7}	9.44×10^{-7}	0.302
7.35	1.49	0.321	-8.75	0.0115	1.83×10^{-7}	1.20×10^{-6}	3.15
5.91	1.32	0.335	-8.78	0.0285	1.30×10^{-4}	1.04×10^{-5}	2.94

Table 5: A selection of four benchmark points represented in Figs. 2, 4 to 6. The $m_{Z'}$, m_{h_2} and x parameters are given in TeV. The first line represents a point with light h_2 while the second line shows the lightest allowed Z' boson found in our scan. The last two lines show two points that reproduce the observed value of the muon $(g-2)$ within 1σ uncertainty.

3.4.1 Implications of direct Z' searches at the LHC for the $(g-2)_\mu$ anomaly

Looking again to Fig. 2 (left panel), we see that there is a thin dark-red stripe where $\Delta a_\mu^{\rm NP}$ explains the observed anomaly shown in Eq. (**??**) for a range of $m_{Z'}$ boson masses approximately between 5 TeV and 20 TeV. This region is particularly interesting as it can be partially probed by the forthcoming LHC runs or at future colliders. If a Z' boson discovery remains elusive for such a mass range, it can exclude a possibility of explaining the muon $(g-2)_\mu$ anomaly in the context of the B-L-SM. It is also worth noticing that such preferred $\Delta a_\mu^{\rm NP}$ values represent a small island in the right plot of Fig. 2 where the new scalar boson mass is restricted to the range of 1 TeV $< m_{h_2} <$ 4 TeV.

New physics contributions $\Delta a_\mu^{\rm NP}$ to the muon anomalous magnetic moment are given at one-loop order by the Feynman diagrams depicted in Fig. 3. Since the couplings of a new

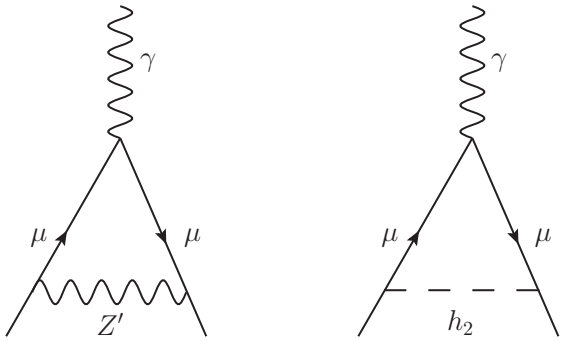

Figure 3: One-loop diagrams contributing to $\Delta a_\mu^{\rm NP}$ in the B-L-SM.

scalar h_2 to the SM fermions are suppressed by a factor of $\sin\alpha_h$, which we find to be always smaller than 0.08 as can be seen in the bottom panel of Fig. 4, the right diagram in Fig. 3, which scales as $\Delta a_\mu^{h_2} \propto \frac{m_\mu^2}{m_{h_2}^2}\left(y_\mu \sin\alpha_h\right)^2$ with $\sin^2\alpha_h < 0.0064$ and $y_\mu = Y_e^{22}$, provides sub-leading contributions to Δa_μ. Furthermore, as we show in the top-left panel of Fig. 4 the

new scalar boson mass, which we have found to satisfy $m_{h_2} \gtrsim 380$ GeV, is not light enough to compensate the smallness of the scalar mixing angle. Conversely, and recalling that all fermions in the B-L-SM transform non-trivially under $\mathrm{U}(1)_{\mathrm{B-L}}$, the new Z' boson can have sizeable couplings to fermions via gauge interactions proportional to $g_{\mathrm{B-L}}$. Therefore, the left diagram in Fig. 3 provides the leading contribution to the $(g-2)_\mu$ in the model under consideration. In particular, $\Delta a_\mu^{Z'}$ is given by [**?**]

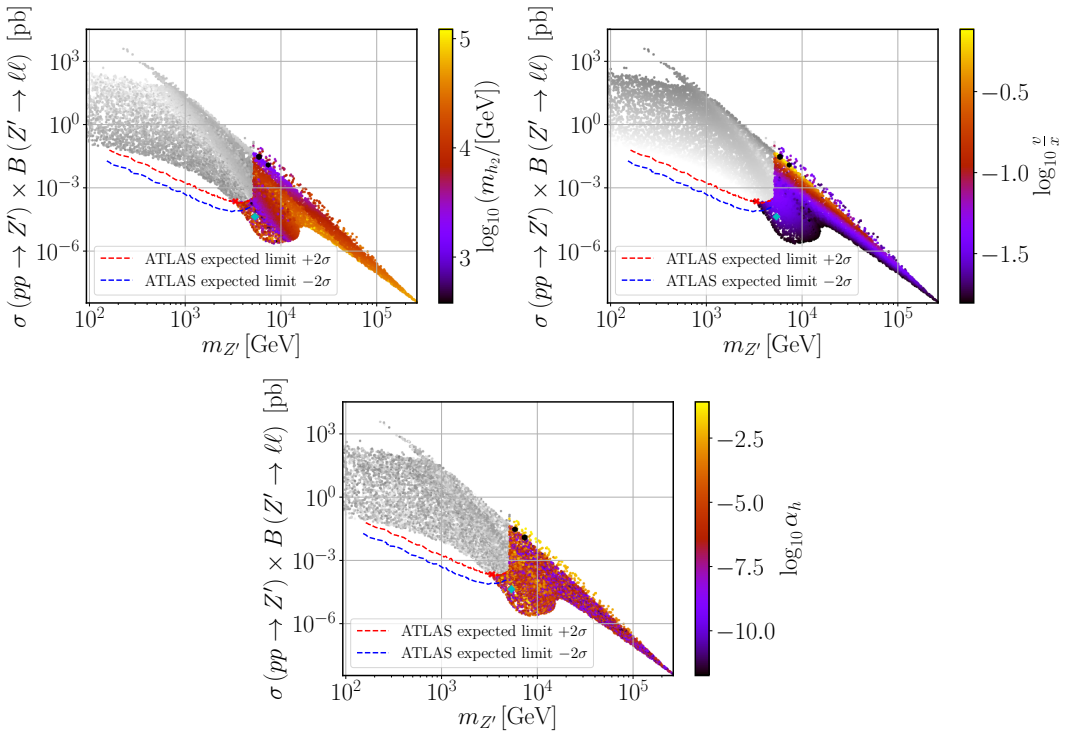

Figure 4: Scatter plots showing the Z' Drell-Yan production cross section times the decay branching ratio into a pair of electrons and muons in terms of the $m_{Z'}$ boson mass. The colour gradation represents the new scalar mass (top-left), the ratio between the EW- and $\mathrm{U}(1)_{\mathrm{B-L}}$-breaking VEVs (top-right) and the scalar mixing angle (bottom). The grey points are excluded by direct Z' searches at the LHC. The four benchmark points in Tab. 5 are represented by the black dots (last two rows), cyan diamond (first row) and red cross (second row).

$$\Delta a_\mu^{Z'} = \frac{1}{12\pi^2}\frac{m_\mu^2}{m_{Z'}^2}\left(3g_{\mathrm{L}}^{\mu\mu Z'}g_{\mathrm{R}}^{\mu\mu Z'} - g_{\mathrm{L}}^{\mu\mu Z'\,2} - g_{\mathrm{R}}^{\mu\mu Z'\,2}\right) \tag{58}$$

where the left- and right-chiral projections of the charged lepton couplings to the Z' boson, $g_{\mathrm{L}}^{\ell\ell Z'}$ and $g_{\mathrm{R}}^{\ell\ell Z'}$, respectively, can be approximated as follows

$$\begin{aligned} g_{\mathrm{L}}^{\ell\ell Z'} &\simeq g_{\mathrm{B-L}} + \tfrac{1}{32}\left(\tfrac{v}{x}\right)^2 \frac{g_{\mathrm{YB}}}{g_{\mathrm{B-L}}}\left[g_{\mathrm{Y}}^2 - g^2 + 2g_{\mathrm{Y}}g_{\mathrm{YB}}\right] , \\ g_{\mathrm{R}}^{\ell\ell Z'} &\simeq g_{\mathrm{B-L}} + \tfrac{1}{16}\left(\tfrac{v}{x}\right)^2 \frac{g_{\mathrm{YB}}}{g_{\mathrm{B-L}}}\left[g_{\mathrm{Y}}^2 + g_{\mathrm{Y}}g_{\mathrm{YB}}\right] , \end{aligned} \tag{59}$$

to the second order in v/x-expansion. If $v/x \ll 1$, corresponding to the darker shades of the

color scale in the top-right panel of Fig. 4, we can further approximate

$$g_{\rm L}^{\ell\ell Z'} \simeq g_{\rm R}^{\ell\ell Z'} \simeq g_{\text{B-L}}\,, \tag{60}$$

such that the muon anomalous magnetic moment gets significantly simplified to

$$\Delta a_\mu^{Z'} \simeq \frac{g_{\text{B-L}}^2}{12\pi^2}\frac{m_\mu^2}{m_{Z'}^2}\,. \tag{61}$$

Similarly, for the yellow band, which corresponds to the region where $\Delta a_\mu^{\rm NP}$ is maximized (see top-left panel of Fig. 2), a large value of the $\mathrm{U}(1)_{\rm B-L}$ gauge coupling also allows one to simplify Eq. (58) reducing it to the form of Eq. (61). This is in fact what we have observed and, for the yellow band region, we see in the bottom panel of Fig. 5 that $g_{\text{B-L}} \simeq 3$. A sizeable value of $g_{\text{B-L}}$ is indeed what is contributing to the enhancement of $\Delta a_\mu^{\rm NP}$, in particular, for the red region in both panels of Fig. 2. We show in the third and fourth lines of Tab. 5 the two benchmark points that better reproduce the muon anomalous magnetic moment represented by two black dots in Figs. 2, 4 to 6.

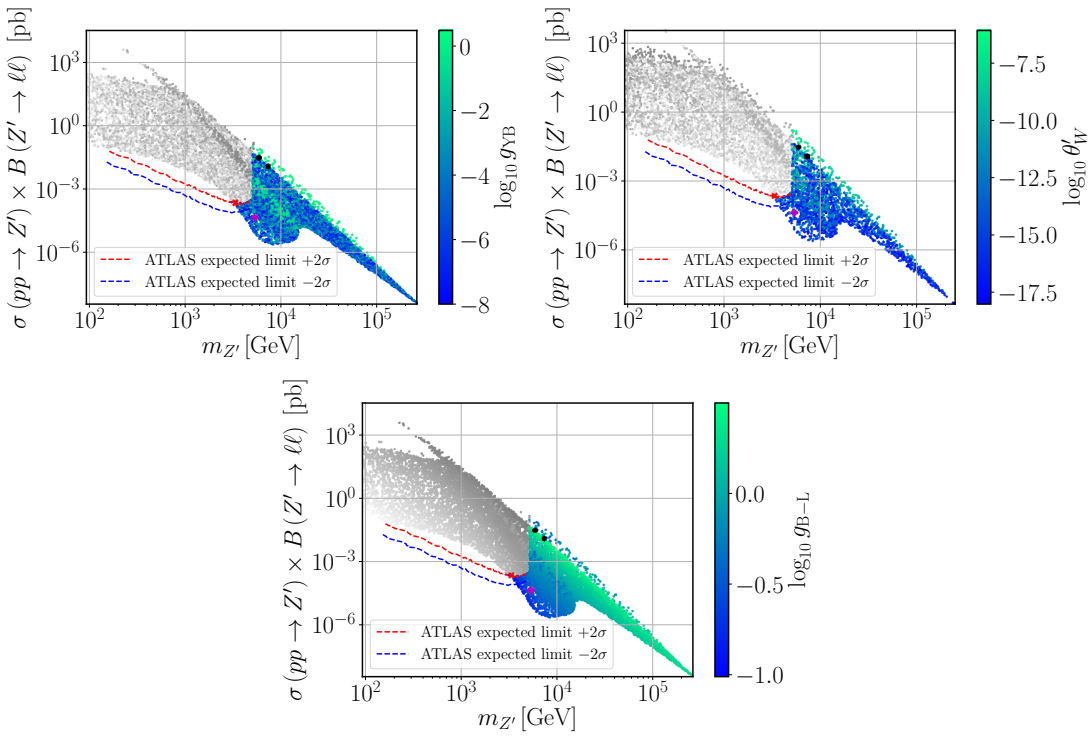

Figure 5: The same as in Fig. 4 but with the colour scale representing the gauge-mixing parameters $g_{\rm YB}$ (top-left) and θ'_W (top-right), and the $\mathrm{U}(1)_{\rm B-L}$ gauge coupling (bottom).

In fact, a close inspection of Fig. 2 (left panel) and Fig. 4 (top-right panel) reveals an almost one-to-one correspondence between the colour shades. This suggests that $\Delta a_\mu^{Z'}$ must somehow be related to the VEV ratio v/x. To understand this behaviour, let us also look to Fig. 5 (top-right panel) where we see that the kinetic-mixing gauge coupling $g_{\rm YB}$ is typically very small apart from two green bands where it can become of order $\mathcal{O}(1)$. Interestingly,

whenever $g_{\rm YB}$ becomes sizeable, $v/x \ll 1$ is realised, which means that Eq. (53) is indeed a good approximation as was argued above. It is then possible to eliminate $g_{\text{B-L}}$ from Eq. (61) and rewrite it as

$$\Delta a_\mu^{Z'} \simeq \frac{y_\mu^2}{96\pi^2}\left(\frac{v}{x}\right)^2 , \tag{62}$$

which explains the observed correlation between both Fig. 2 (left panel) and Fig. 4 (top-right panel) and, for instance, the thin red stripe of points compatible with a full description of the muon $(g-2)_\mu/2$ anomaly. Note that this simple and illuminating relation becomes valid as a consequence of the heavy Z' mass regime, in combination with the smallness of the θ'_W mixing angle required by LEP constraints. Indeed, while we have not imposed any strong restriction on the input parameters of our scan (see Tab. **??**), Eq. (49) necessarily implies that both $g_{\rm YB}$ and v/x cannot be simultaneously sizeable in agreement with what is seen in Fig. 5 (top-left panel) and Fig. 4 (top-right panel). The values of θ'_W obtained in our scan are shown in the top-right panel of Fig. 5.

For completeness, we show in Fig. 6 the physical couplings of Z' to muons (top panels) and to $W^\pm$ bosons (bottom panel). Note that, for the considered scenarios, the latter can be

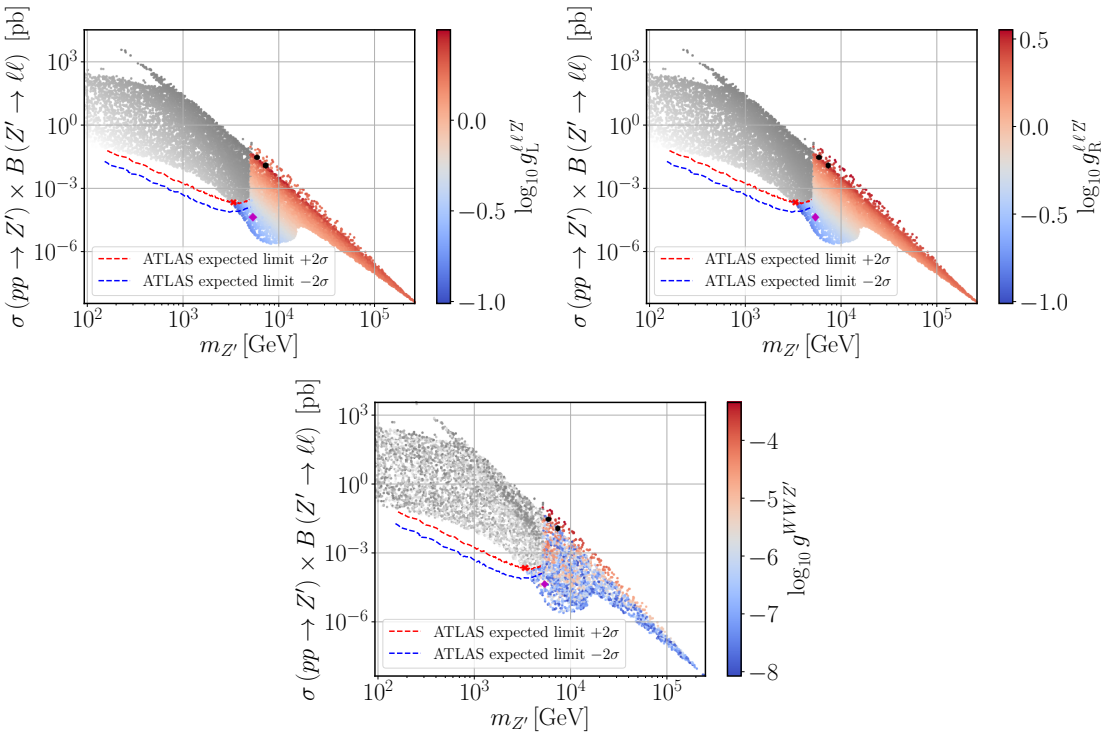

Figure 6: The same as in Fig. 4 but with the colour scale representing the coupling of leptons to the Z' (top panels) and the coupling of W bosons to Z'.

written as

$$g^{WWZ'} \simeq \frac{1}{16}\frac{g_{\rm YB}}{g_{\text{B-L}}}\left(\frac{v}{x}\right)^2 . \tag{63}$$

While both $g_{\text{B-L}}$ and the ratio v/x provide a smooth continuous contribution in the $\sigma B - m_{Z'}$ projection of the parameter space, the observed blurry region in $g^{WWZ'}$ is correlated with the one in the top-left panel of Fig. 5 as expected from Eq. (63). On the other hand, the

couplings to leptons $g^{\ell\ell Z'}_{\rm L,R}$ exhibit a strong correlation with $g_{\rm B\text{-}L}$ in Fig. 5, in agreement with our discussion above and with Eq. (60).

3.4.2 Barr-Zee type contributions

To conclude our analysis, one should note that the two-loop Barr-Zee type diagrams [**?**] are always sub-dominant in our case. To see this, let us consider the four diagrams shown in Fig. 7. The same reason that suppresses the one-loop h_2 contribution in Fig. 3 is also

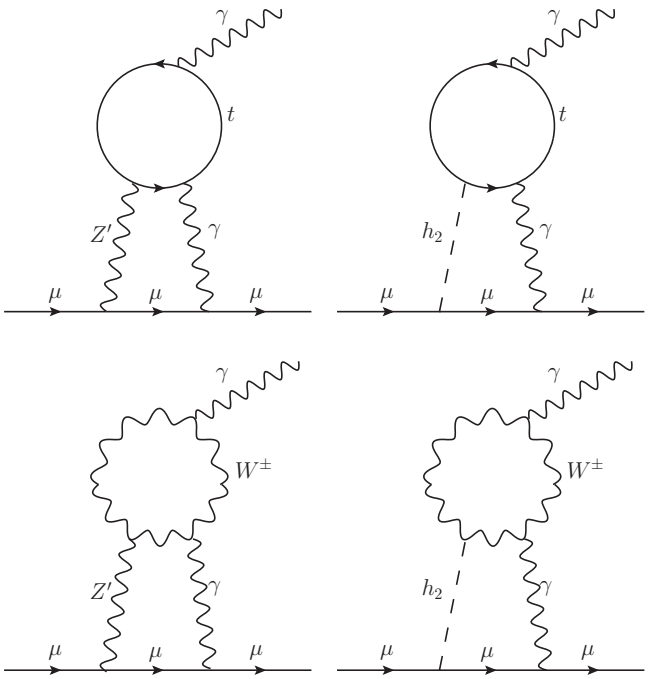

Figure 7: Barr-Zee type two-loop diagrams contributing to Δa_μ.

responsible for the suppression of both the top-right and bottom-right diagrams in Fig. 7 (for details see e.g. Ref. [**?**]). Recall that the coupling of h_2 to the SM particles is proportional to the scalar mixing angle α_h, which is always small (or very small) as we can see in Fig. 4. An analogous effect is present in the diagram involving a W-loop, where a vertex proportional to $g^{WWZ'}$ suppresses such a contribution. The only diagram that might play a sizeable role is the top-left one where the couplings of Z' to both muons and top quarks are not negligible.

Let us then estimate the size of the first diagram in Fig. 7. This type of diagrams were already calculated in Ref. [**?**] but for the case of a SM Z-boson. Since the same topology holds for the considered case of B-L-SM too, if we trade Z by the new Z' boson, the contribution to the muon $(g-2)_\mu$ anomaly can be rewritten as

$$\Delta a_\mu^{\gamma Z'} = -\frac{g^2 g_{\rm B\text{-}L}^2 m_\mu^2 \tan^2\theta_W}{1536\pi^4}\left(g_{\rm L}^{ttZ'} - g_{\rm R}^{ttZ'}\right) {\rm T}_7\left(m_{Z'}^2, m_t^2, m_t^2\right) , \tag{64}$$

where $g^{ttZ'}_{\rm L,R}$, calculated in `SARAH`, are the left- and right-chirality projections of the Z' coupling

to top-quarks, given by

$$
\begin{aligned}
g_{\mathrm{L}}^{ttZ'} &= -\frac{g_{\text{B-L}}}{3}\cos\theta'_W + \frac{g}{2}\cos\theta_W\sin\theta'_W - \frac{g_{\mathrm{Y}}}{6}\sin\theta_W\sin\theta'_W - \frac{g_{\mathrm{YB}}}{3}\sin\theta_W\sin\theta'_W\,, \\
g_{\mathrm{R}}^{ttZ'} &= -\frac{g_{\text{B-L}}}{3}\cos\theta'_W - \frac{2g_{\mathrm{Y}}}{3}\sin\theta_W\sin\theta'_W - \frac{g_{\mathrm{YB}}}{3}\sin\theta_W\sin\theta'_W\,.
\end{aligned}
\tag{65}
$$

The loop integral $\mathrm{T}_7\left(m_{Z'}^2, m_t^2, m_t^2\right)$ was determined in Ref. [**?**] and, in the limit $m_{Z'} \gg m_t$, as we show in Eq. (**??**), it gets simplified to

$$
\mathrm{T}_7\left(m_{Z'}^2, m_t^2, m_t^2\right) \simeq \frac{2}{m_{Z'}^2}\,, \tag{66}
$$

up to a small truncation error (see Appendix **??** for details). For the parameter space region under consideration the difference $g_{\mathrm{L}}^{ttZ'} - g_{\mathrm{R}}^{ttZ'}$ can be cast in a simplified form as follows

$$
\left(g_{\mathrm{L}}^{ttZ'} - g_{\mathrm{R}}^{ttZ'}\right) \simeq \frac{\left(g^2 + g_{\mathrm{Y}}^2\right) g_{\mathrm{YB}}}{32 g_{\text{B-L}}}\left(\frac{v}{x}\right)^2\,. \tag{67}
$$

Using this result and the approximate value of the loop factor, we can calculate the ratio between the two- and one-loop contributions to the muon $(g-2)_\mu$,

$$
\frac{\Delta a_\mu^{\gamma Z'}}{\Delta a_\mu^{Z'}} \simeq -\frac{g^2 g_{\mathrm{Y}^2}}{2048\pi^2}\frac{g_{\mathrm{YB}}}{g_{\text{B-L}}}\left(\frac{v}{x}\right)^2 \ll 1\,, \tag{68}
$$

which shows that $\Delta a_\mu^{\gamma Z'}$ does indeed play a subdominant role in our analysis and can be safely neglected.

3.5 Conclusion

To summarise, in this work we have performed a detailed phenomenological analysis of the minimal $\mathrm{U}(1)_{\mathrm{B-L}}$ extension of the Standard Model known as the B-L-SM. In particular, we have confronted the model with the most recent experimental bounds from the direct Z' boson and next-to-lightest Higgs state searches at the LHC. Simultaneously, we have analysed the prospects of the B-L-SM for a consistent explanation of the observed anomaly in the muon anomalous magnetic moment $(g-2)_\mu$. For this purpose, we have explored the B-L-SM potential for interpretation of the $(g-2)_\mu$ anomaly in the regions of the model parameter space that are consistent with direct searches and electroweak precision observables.

As one of the main results of our analysis, we have found phenomenologically consistent model parameter space regions that simultaneously fit the exclusion limits from direct Z' searches and can explain the muon $(g-2)_\mu$ anomaly. In particular, we have identified four benchmark points for future phenomenological exploration – the first one with the lightest Z' ($m_{Z'} > 3.1$ TeV), the second – with the lightest second scalar boson ($m_{h_2} > 400$ GeV), and the other two points that reproduce the muon $(g-2)_\mu$ anomaly within 1σ uncertainty range. Besides, we have studied the correlations of the Z' production cross section times the branching ratio into a pair of light leptons versus the physical parameters of the model. In particular, we have found that the muon $(g-2)_\mu$ observable dominated by Z' loop contributions lies within the phenomenologically viable parameter space domain. For completeness, we have also estimated the dominant contribution from the Barr-Zee type two-loop corrections and found a relatively small effect.

4 3HDM

Let us now consider an extended version of the SM, with an enlarged Higgs sector that contains three generations of scalar-doublets. These Higgs will be named ϕ^i with $i = 1, 2, 3$.

5 Conclusions and Future Work

6 Appendix

6.1 Gamma Matrices

The γ matrices are defined as,

$$\{\gamma^\mu, \gamma^\nu\} = 2g^{\mu\nu} I \tag{69}$$

where,

$$g^{\mu\nu} = \begin{pmatrix} 1 & 0 & 0 & 0 \\ 0 & -1 & 0 & 0 \\ 0 & 0 & -1 & 0 \\ 0 & 0 & 0 & -1 \end{pmatrix} \tag{70}$$

and if $\gamma_\mu = (\gamma^0, \gamma)$ then it is usual to require for the hermitian conjugate matrices,

$$\gamma^{0\dagger} = \gamma^0 \quad \text{and} \quad \gamma^\dagger = -\gamma \tag{71}$$

6.2 Lagrangian Dynamics

In Lagrangian dynamics we define the action S has,

$$\mathcal{S} = \int L\, dt = \int \mathcal{L}(\phi, \partial\phi)\, d^4x \tag{72}$$

where L is the Lagrangian, and the $\mathcal{L}$ is designated as the *Lagrangian density*, note these terms are usually used interchangeable. Here $\mathcal{L}$ is a function of the field ϕ and it's spatial derivatives.

The action S is constrained by the principle of least action, this requires the "path" taken by a field between an initial and final set of coordinates to leave the action invariant, this can be expressed by,

$$\partial\mathcal{S} = 0 \tag{73}$$

from here one can deduce the *Euler-Lagrange* equations,

$$\partial_\mu \left(\frac{\partial\mathcal{L}(\phi, \partial\phi)}{\partial(\partial_\mu)} \right) - \frac{\partial\mathcal{L}(\phi, \partial\phi)}{\partial\phi} = 0 \tag{74}$$